Kirigami-inspired stents for sustained local delivery of therapeutics

Kirigami-inspired stents for sustained local delivery of therapeutics

Sahab Babaee[1,2,3], Yichao Shi[1], Saeed Abbasalizadeh[1], Siddartha Tamang[1], Kaitlyn Hess[1], Joy E. Collins[1,3], Keiko Ishida[1], Aaron Lopes[1], Michael Williams[1,2], Mazen Albaghdadi[1,4], Alison M. Hayward[1,3], Giovanni Traverso[1,2,3]*

[1]Department of Mechanical Engineering, Massachusetts Institute of Technology, Cambridge, MA 02139, USA.
[2]Department of Chemical Engineering and Koch Institute for Integrative Cancer Research, Massachusetts Institute of Technology, Cambridge, MA 02139, USA.
[3]Division of Gastroenterology, Brigham and Women's Hospital, Harvard Medical School, Boston, MA 02115, USA.
[4]Division of Cardiology, Massachusetts General Hospital, Harvard Medical School, Boston, MA 02115, USA.

*Corresponding author. E-mail: cgt20@mit.edu (G.T.)

Abstract: Implantable drug depots have the capacity to locally meet therapeutic requirements by maximizing local drug efficacy and minimizing potential systemic side effects. Tubular organs including the gastrointestinal tract, respiratory tract and vasculature all manifest with endoluminal disease. The anatomic distribution of localized drug delivery for these organs using existing therapeutic modalities is limited. Application of local depots in a circumferential and extended longitudinal fashion could transform our capacity to offer effective treatment across a range of conditions. Here we report the development and application of a kirigami-based stent platform to achieve this. The stents comprise a stretchable snake skin-inspired kirigami shell integrated with a fluidically-driven linear soft actuator. They have the capacity to deposit drug depots circumferentially and longitudinally in the tubular mucosa of the GI tract across millimeter to multi-centimeter length scales, as well as in the vasculature and large airways. We characterize the mechanics of kirigami stents for injection, their capacity to engage tissue in a controlled manner and deposit degradable microparticles loaded with therapeutics by evaluating these systems *ex vivo* and *in vivo* in swine. We anticipate such systems could be applied for a range of endoluminal diseases by simplifying dosing regimens while maximizing drug on target effect through the sustained release of therapeutics and minimizing systemic side effects.

One Sentence Summary: Kirigami-inspired stent-based systems enable extended local drug release through deposition of drug-loaded polymeric particles to the gastrointestinal tract, respiratory tract, or any tubular organ in the body.

Main

Implantable drug depots have been applied for decades across a range of sites in the body including the brain[1]. For tubular structures in the body such as the gastrointestinal (GI) system, airways, and vasculature, the targeted delivery of therapeutics remains challenging. In patients with enteral and respiratory malignancies, uncoated stents provide mechanical scaffolding of the obstructed luminal structure but do not provide release of antiproliferative agents that can reduce tissue in-growth associated with stent failure[2,3]. Eosinophilic esophagitis and Inflammatory bowel disease (IBD) may also benefit from novel local drug delivery strategies designed to achieve high drug concentrations at the site of inflammation with minimal exposure of healthy or distant tissues and to avoid immunosuppressive effects of systemic drugs commonly used to treat IBD[4]. Endoluminal drug delivery systems such as drug-eluting stents and drug-coated balloons are effective at providing high local concentrations of anti-proliferative agents and reducing vascular renarrowing (or restenosis) in vessels affected by obstructive atherosclerosis[5,6]. However, existing drug-coated balloons are limited in efficacy due to the limited transfer and retention of drug from the balloon to vessel wall and thus novel local delivery systems are needed.

In the GI tract, the clinical potential of coated stents is limited by a significant rate of complications including stent migration and tissue perforation[7,8]. Moreover, the delivery from drug eluting stents is governed by diffusion limitations through tissue potentially limiting delivery to therapeutics of lower molecular weight and particular physico-chemical characteristics of target tissues which support partitioning of the drug into the mucosa. In the GI tract endoscopic injection, initially pioneered through the development of endoscopy-guided injection needles[9] transformed the capacity to locally deliver therapeutics for a range of indications including hemostasis with epinephrine[10], sclerosant injection for variceal ablation[11], submucosal lifts with normal saline and other materials[12], as well as steroid injections for inflammation control[13], and injection of biologics for inflammatory stricture management[14]. All these applications mainly apply a hypodermic needle that can be deployed endoscopically supporting single site injection. Recognizing that many GI pathologies including inflammatory bowel disease, eosinophilic GI disorders, and celiac disease frequently affect extended multi-centimeter segments of the GI tract, we aimed to develop a solution that could provide rapid circumferential and longitudinal submucosal deposition of controlled drug releasing systems. To do this we developed a kirigami-mediated drug depositing stent system.

Kirigami – the Japanese form of paper art similar to origami that includes cutting of the paper – has recently enabled the design of a range of novel functional tools and programmable systems from macroscale soft actuators and robots[15,16] to microelectronics[17,18] and nanostructures[19-22]. Buckling-induced kirigami structures are engineered to utilize local elastic instabilities for versatile shape transformation from flat to complex three-dimensional (3D) architectures[23-25]. Recently, the buckling kirigami metasurfaces have been applied to footwear outsoles to generate higher friction forces and mitigate the risk of slips and falls in a range of environments[26]. Here, inspired by the skin of scaly-skin animals like snakes and sharks, we developed a drug-depositing stent composed of a periodic array of denticle-like needles (i.e., a kirigami cylindrical shell) integrated with a pneumatic soft actuator. Through a combination of finite element (FE) simulations and experiments, we identified kirigami shells and linear actuators to inform the development of drug-depositing stents in multiple length scales that can be easily deployed in the tubular lumen of tubular structures of various diameters including esophagus, blood vessels, and airways. Importantly, we demonstrated that by pressurizing the soft actuator, the kirigami needles are forced to buckle outward such that they undergo a change in orientation from planar to perpendicular to the stent body surface. The radial expansion of the device, up to 60% of the stent diameter, enabling submucosal injections of drug-loaded degradable microparticles. These kirigami-based injectable stents could serve as a new class of local drug-releasing systems, capable of deploying drug depots through multi-point deposition of drug particles directly into luminal walls, thereby enhancing sustained local delivery of therapeutics. Furthermore, recognizing many tubular organs in the body in addition to the GI tract, we demonstrated in vivo and ex vivo the capacity of the system to interface with the respiratory and vascular systems.

Design of gastrointestinal kirigami-inspired stents

Figure 1A shows the schematic of the kirigami-based stent composed of two building components. First, a cylindrical kirigami skin consists of a periodic array of snake denticle-like cuts embedded in thin plastic sheets (see Supplementary Methods and Supplementary Figure 1A). The cuts are in the form of a triangular arrangement of barb-shaped needles with the cut angle $\gamma = 30°$ and the dimensionless ratio $\delta/l = 0.13$ where δ is the width of the ligaments separating the cuts and l is the characteristic length of the periodic pattern considered as needle length (Figure 1A, inset). These parameters have been shown to allow a pop-out deformation of kirigami surfaces upon stretching[15,23,26]. The second component is a pneumatic fiber-reinforced soft actuator made of a 1.5 mm thick silicone-based rubber (see Supplementary Methods and Supplementary Figure 1B) that can provide a linear motion to induce tensile strain in the kirigami skin and trigger the needles to pop out. The radial expansion (ε^r) and axial extension (ε^a) of the stent and popping angle of the needles (θ) can be tuned by controlling the actuator pressure (P/P_0), where P_0 =1 atm. For example, ε^r and θ are monotonically increased through applying external pressure for the illustrated stent design (Figure 1A, inset plot). The kirigami stent can be manufactured in various sizes to be placed endoscopically in the GI tract across multi-centimeter length scales as well as in the vasculature, and airways. Figure 1B shows a schematic of the stent deployed in the lumen of the

esophagus, intestine, trachea, and iliac artery. The needles can be coated with drug particles to enable the local delivery of therapeutics through circumferential injections.

The deformation response of the kirigami stents can be controlled by varying the thickness of the kirigami shell (t) and the needle length (l) as a function of applied pressure. We constructed numerical models of the kirigami stents with different combinations of t and l, and employed non-linear finite elements (FE) analyses to capture the deformation of the stents subjected to the applied actuator pressure using the commercial FE package Abaqus/Explicit (see Methods and Supplementary Video 1). We aimed to identify an optimal stent design that exhibits larger radial expansion (ε^r) and higher out-of-plane stiffness of the needles (K^{33}) for better engagement with the surrounding tissue and injection while actuated.

We carried out a systematic study to predict the effect of t and l on the evolution of ε^a, ε^r, and θ as a function of the applied actuator pressure (P/P_0) for an esophageal-sized stent with $L_0 = 8$ cm and $D_0 =$ 12.5 mm. The summary of those data was presented in the color maps shown in Figure 1C, where we reported the actuator pressure $P_{\max}/P_0$ (panel I) required to achieve corresponding ε^a_{max} (panel II), ε^r_{max} (panel III), and θ_{max} (panel IV) of the stent. We specifically explored geometrical parameters ranging from t = 0.05, 0.08, 0.10, 0.13, 0.19 mm and l = 3.0, 4.8, 6.7, and 10.0 mm. The data clearly indicate that by increasing l, ε^r_{max} considerably rises, and ε^a_{max}, θ_{max}, and $P_{\max}/P_0$ slightly increase for a given t (Supplementary Figure 2 and Supplementary Video 2). Therefore, l = 10.0 mm was selected as a good candidate for needle length to achieve maximum radial expansion. Furthermore, by increasing t, $P_{\max}/P_0$ increases at constant l, however, ε^a_{max}, ε^r_{max}, and θ_{max} are almost remained unaltered (Supplementary Figure 3 and Supplementary Video 3).To identify the proper t, we fabricated kirigami surfaces with various thicknesses (see Methods), and experimentally investigated the effect of t on the stiffness of the kirigami needles in the normal direction, denoted by K^{33} (see Supplementary Method). It demonstrated that increasing t, significantly increases the out-of-plane stiffness of the needles (Supplementary Figure 4). Therefore, choosing a thicker kirigami could result in stiffer needles that could potentially provide easier penetrations. Since the kirigami with the maximum thickness (t =0.19 mm in grey) shows localized plastic zones at the hinges that slightly affects the reversible deformation of the needles (i.e., return to the initial flat configuration after releasing the load) needed for safe removal, we selected the kirigami with t =0.13 mm as a desired candidate for making the kirigami shell. Having identified l = 10.0 mm and t =0.13 mm as ideal design parameters that provide simultaneous highest ε^r and K^{33}, we proceeded to fabricate the stent prototypes and experimentally evaluated the performance.

The schematic visualization of the fabrication process is illustrated in Figure 2A. The linear actuator is a soft fluid-powered fiber-reinforced actuator consists of multiple segments[27]. A cylindrical elastomeric tube – fabricated from a silicon-based rubber using a casting approach – is surrounded by Kevlar fibers arranged in a helical pattern at a characteristic fiber angle $\beta = 10°$ and sealed at both ends. A 20G blunt needle with a plastic plug was incorporated to the one end used for transferring fluid pressure (i.e., actuation) via a tubing. The soft actuator can produce a linear motion (i.e., extension) up to 0.5 axial strain when pressurized (see Methods, Supplementary Figure 5 and Supplementary Video 4). The kirigami surface is a patterned array of barb-shaped needles that can be easily cut when it is flat, and then glued into a cylindrical shell (Supplementary Figure 6). Note that the plastic kirigami surfaces are hydrophobic and have a poor adhesion bond to drug-coated films. Air plasma treatment was utilized to micro clean and alter the surface properties of the kirigami surfaces for adhesion improvement (see Methods). To further enhance the adhesion between the plastic surface and the coating layer, the external surface area of the needles was laser engraved with six raster lines (0.5 mm spacing) when it is flat. Lastly, the linear actuator was inserted into the cylindrical shell and both ends were glued. The key feature of the kirigami shell (or stent) is capable of reversible shape transformation from flat configuration (for device delivery and removal) to 3D surfaces with popped-up needles (for injections) that enables facile delivery, robust deployment, and safe removal of the drug-releasing system (see Supplementary Methods, and Supplementary Figure 7).

In Figure 2B**,** we report the experimental snapshots of the esophageal stent prototype at different levels of actuator pressure, $P = 1.0$, 1.5, 2.7, 3.4, 4.4, and 5.2 atm, where $P = 1.0$ and 5.2 atm correspond to undeformed and fully deployed configurations, respectively. The esophageal stent has an initial length

$L_0 = 8$ cm and outer diameter $D_0 = 12.5$ mm that ensures the safe delivery of the stent to the esophagus (with >15 mm inner diameter) under endoscopic guidance. The surrounding kirigami shell has 26 barb-shaped needles with l = 10.0 mm and $t = 0.13$ mm (the ideal design parameters, Supplementary Figure 6A). The experimental images are compared to the numerical snapshots obtained from non-linear FE simulations, showing that the kirigami shell is initially flat and then transform into 3D configurations with buckled out needles upon pressurizing the actuator. By releasing the pressure, the needles are popped in and recovered their original undeformed shape (Supplementary Video 5). We quantified the deformation of the prototype and compared the experimental data (blue markers) to the FE results (red dashed lines), showing a close agreement. We reported the evolution of axial extension ($\varepsilon^a = L/L_0$), radial expansion ($\varepsilon^r = D/D_0$), and popping angle (θ) as a function of the actuator pressure (P/P_0) in Figure 2C, demonstrating a gradual linear increase in ε^a, ε^r, and θ due to out-of-plane buckling of needles, and then a plateau at higher pressure up to $P/P_0 = 6.5$ results in $\varepsilon^a_{max} = 0.36$, $\varepsilon^r_{max} = 0.57$, and $\theta_{max} = 28°$. This considerable expansion of the stent especially in the radial direction allows a close engagement of the popped-up needles against the mucosa. Finally, to ensure the ability to fabricate the stents in multiple sizes and consistency with our numerical prediction, we fabricated further esophageal stents with multiple combinations of t and l, and monitored their deformation using both FE simulations and experiments, showing an excellent qualitative agreement (see Supplementary Videos 6 and 7**,** and Supplementary Figure 8).

Controlled penetration of stent needles to the GI mucosa

Micro-computed tomography (micro-CT) imaging and histology from ex vivo and in vivo experiments have been employed to demonstrate that the stent needles can be inserted by more than 1 mm into the submucosa of swine esophageal tissue without causing perforation. The penetration depth of the needles (d) can be controlled by incorporating the arc-shaped features (i.e., dimples with $R = 1.5$ mm) on the two sides of the needles, shown in Figure 3A. These small features could stop further penetration when contacting the tissue surface. We positioned the dimples at a characteristic distance H from the tip of the needles. We considered H = 1.5, 2.5, 3.5 mm, and no dimple (control) corresponds to needle 1 (blue), needle 2 (green), needle 3 (orange), and needle 4 (black), respectively. To quantify d, we started by in vitro deployment of the stents brushed with a thin layer of tungsten filled radio-opaque ink in the esophagi harvested from Yorkshire pigs using a custom 3D printed fixture (see Methods, $n = 4$). Figure 3A shows the representative 3D micro-CT image of the deployed stent and 2D cross-sectional slices used to obtain d. The data were reported in the plot, showing d = 0.549 ± 0.092, 0.914 ± 0.156, 0.926 ± 0.176, and 0.932 ± 0.148 mm for the stents made of needle 1, needle 2, needle 3, and needle 4, respectively (mean ± SD, n ≥ 10).

Note that all the needles penetrated into tissues with an average tilting angle $\theta \sim 22°$, which is the maximum popping angle (considering the surrounding tissue wall) achieved by pressurizing the soft actuator up to $P_{\max}/P_0 = 6.5$ and gently pulling it backward via application of ~8 N force. Therefore, the maximum penetration depths (d_{max}) were predicted as $d_{max} = H \sin\theta = 0.57$, 0.96, and 1.34 mm for the needles 1 to 3 (dashed lines in Figure 3A plot). For the needles 1 and 2, the experimental results matched with the predicted d_{max} verifying that the dimples were able to stop the insertion of the needles. However, the needle 3 does not reach d_{max}, demonstrating that for the given 8 N pulling force, the penetration depth of needle 3 is equivalent to the control needle 4 that has no dimple. To ensure the safety margin on the insertion depth, we deployed the kirigami stent in vivo (see Methods), and performed histological image analysis of the esophageal tissues at the penetration sites, showing $d = 1.09 \pm 0.16$ mm without perforation when we applied 8 N force (mean ± SD, $n = 5$**,** see Figure 3B and Methods). Similar kirigami-based stents of a size compatible with the anatomic compartment and needle stiffness were prototyped to demonstrate the ability of circumferential injections in other tubular parts of the body including femoral arteries (see Methods) and trachea. The endovascular stent has initial length $L_0 = 7$ cm and outer diameter $D_0 = 5.5$ mm (Supplementary Figure 9), and the tracheal stent has $L_0 = 8$ cm and outer diameter $D_0 = 15$ mm (Supplementary Figure 10). For all the experiments, the kirigami stents were kept in place in the deployed configuration with popped-up needles for a period of two minutes and then returned to its delivery configuration and removed from the body lumen.

In vivo delivery of fluorescent polystyrene microparticles

To enable loading and delivery of polymeric particles with the injectable stent system, we coated the external surface of the stent (i.e., kirigami shell) with a solution of fluorescent magnetic polystyrene microparticles (4.0-4.9 μm nominal size, see Methods). A custom-built benchtop spray coating set-up with programmable stent movement and rotation was used to achieve a uniform thin film coating of the solution onto the kirigami stent shell (see Supplementary Methods, Supplementary Figure 11, and Supplementary Video 8). The fluorescent magnetic microparticles were delivered in vivo in three porcine esophagi using the coated prototypes (Figure 3, C and D), clearly demonstrating a periodic array of higher fluorescent concentration spots at the kirigami needle penetration sites, further supporting the potential for this drug delivery system to administer polymeric particles to the GI tract (see Methods). The optimal penetration depth and distance between the penetration sites would be guided by disease activity indices and clinical trials.

In vivo sustained drug release

To evaluate the performance of the kirigami stents for extended drug release, we conducted in vivo studies in swine using budesonide as a model drug. We demonstrated that the transiently placed stent delivered drug depots capable of releasing drug for up to a week through multipoint submucosal deposition of drug-loaded degradable particles in the tissue. Budesonide, an anti-inflammatory drug commonly used to treat inflammatory bowel disease and eosinophilic GI disorders, was encapsulated into poly lactic-*co*-glycolic acid (PLGA) degradable microparticles with high concentrations using continuous microfluidic droplet generation method. We synthesized three formulations of budesonide loaded PLGA particles with 75,100, and 125 mg/ml concentration of budesonide, denoted by BUD 75, BUD 100, and BUD 125, respectively. Additionally, we synthesized 100 mg/ml concentration of fluorescent budesonide-PLGA particles (BUD 100F) via the addition of a fluorescent agent (see Methods, and Supplementary Figure 12). Figure 4A shows the morphological characteristics of the synthesized drug particles for the different formulations, exhibit budesonide encapsulated into PLGA microspheres for BUD 75, BUD 100, BUD 125, and BUD 100F (see Methods and Supplementary Figure 13). Drug release occurs through polymeric microparticles erosion and diffusion from the polymer matrix during retention in tissue. The in vitro release kinetics of budesonide from the PLGA particles in phosphate-buffered saline (PBS) were analyzed using High-Performance Liquid Chromatography (see Methods). Notably, the release profile of encapsulated budesonide demonstrated an initial burst release followed by linear drug release up to approximately 40% across all the formulations over 7 days of incubation in PBS at 37°C (Figure 4B).

We loaded the needle surfaces including the tips of the kirigami stents by pipetting 20 μl of the BUD 100F particle solution two times per needle with a 5 h interval for drying at room temperature (see Methods). Figure 4C shows the coated kirigami stent and the magnified view of a needle surface/tip taken by a fluorescence microscope, showing consistent deposition of a uniform budesonide-PLGA microparticles layer onto the stent surface. Three esophageal kirigami stents with drug-loaded polymeric particles were delivered in vivo to the middle and distal esophagus of a large animal model (three Yorkshire pigs), temporarily expanded and engaged with the submucosal wall via multipoint circumferential penetration of the kirigami needles, and deposited drug particles. The kirigami needles were left in place in the popped-up configuration for two minutes. After the prescribed residence time the device is returned to its delivery configuration and removed from the treated body lumen (see Methods and Supplementary Video 9). The two-minute residence time allows for the drug particles to be deposited from the external surface of the needles into the GI submucosa. Note that the system is not ingested or implanted rather it delivers the payload and is then removed (acutely). The payload is left in the submucosa of the targeted wall to provide extended release. The animals were euthanized at different time points: 1 day, 3 days and 7 days after delivery, and their esophagi harvested to extract budesonide and analyzed using ultraperformance liquid chromatography-tandem mass spectrometry (UPLC-MS/MS) (see Methods). The concentrations of budesonide delivered using the injectable stents are reported in Figure 4D. Remarkably, the data indicate that we were able to detect budesonide up to $0.09 \pm 0.02\ \mu g/g$ per mass of tissue even after 7 days of the delivery associated with rapid absorption of the drug in the tissue, enabling sustained local delivery of budesonide and supporting the potential for this controlled drug releasing system to deliver drug agents to the tubular segments of GI tract.

Discussion

In summary, given the recognized capacity for disease treatment from local drug depots, we aimed to develop a new class of biomedical device(s) that support the deployment of drug releasing systems through a multipoint injection for tubular organs. Our objective was addressed by the following: First, design, FE modeling, prototyping a kirigami-based stent platform and characterizing the mechanics for robust deployment, multi-point injection, and safe removal in the tubular mucosa of the GI tract. Second, in vivo evaluation of the capacity to deposit drug-loaded polymeric particles for extended release using a large animal model. To develop the kirigami stent, first, buckling-induced kirigami surfaces were engineered to undergo a shape transformation from flat surfaces to 3D textured surfaces with popped-up needles. By turning kirigami surfaces to cylindrical kirigami skins, we presented a systematic study through combining FE simulations and experiments to investigate the effect of kirigami mesostructure (needle length and thickness) on the mechanical response of kirigami shells. Next, a fluid-powered elastomeric actuator was employed to generate linear output motion using a simple control input (i.e., pressurization of a working fluid) to trigger the kirigami shell for drug deposition. Importantly, we demonstrated that combining kirigami design principles and the fluidic soft actuator provides a new way to deliver drug depots locally and could potentially be used to administer other APIs. Altogether, our design of an injectable kirigami stent offers a unique mechanism with a range of advantages: It can be applied to various length-scales to be matched with the size of the target tubular compartments of the GI tract, vasculature, and airways. It can rapidly deploy by more than 50% radial expansion and release therapeutics into submucosa through circumferential injections, and it demonstrates shape recovery to the original flat configuration by releasing the actuator pressure for safe removal.

Here we demonstrate the capacity to rapidly deploy extended drug release depots in luminal segments of the body with a particular focus on the esophagus. Such systems have the capacity to provide long term local therapy for chronic conditions whilst minimizing the actual need to take a medication thereby potentially maximizing adherence. Moreover, the ability to provide targeted extended drug release stands to mitigate systemic drug affects and also potentially maximize high local concentrations of the therapeutic. The kirigami stent is not ingested or implanted rather it delivers the payload though transient deployment into the lumen for a period of minutes and is then removed (acutely). The payload is left in the submucosa of the wall to provide extended release as a new way of managing luminal diseases including eosinophilic esophagitis, inflammatory bowel disease, and potentially other conditions which can benefit from local depots. The deployment method is a minimally invasive outpatient procedure via transluminal or endoluminal (e.g., transesophageal or transtracheal) access under local anesthesia. Moreover, the local therapeutic delivery of radiofrequency and photodynamic therapies for malignant and pre-malignant GI tumors is routinely performed clinically. Thus, the logistics for local delivery of the kirigami stents has precedent in clinical practice. Certain parts of the body might not be easily accessible for stent insertion, e.g. the jejunum. This point is a limitation in this study and a potential area of future extended local drug delivery systems, which would require extended endoscopic procedures such as double-balloon enteroscopy.

Plasma treatment of the stent surface that improves the hydrophilicity of plastic kirigami surfaces, combined with laser engraving the needle surfaces to increase surface area were used as two key post-treatment techniques to improve adhesion bond between the coating layer (drug-particle solution) and kirigami stents needles that consequently enhance drug loading capacity. However, we may lose some drug particles by potential washing off the stent during delivery. This could be more pronounced in the vasculature in the presence of blood flow. Further studies employing various polymeric surface textures to enhance drug loading capacity as well as polymeric sacrificial layers to protect the drug-coated particles, can be performed to increase drug loading capacity. Sacrificially protected delivery is expected to decrease loss of drug particles leading to increased delivery of drug payload. Utilizing an introducer sheath will also protect the stent during delivery and eliminate the need for a separate introducer for facile delivery. In our study we demonstrated the capacity to deposit microparticles capable of releasing budesonide over the course of several days. Further efficiency and localization of the drug could be introduced through selective coating of the needles thereby minimizing materials that remain in the lumen. This potentially opens new avenues in developing improved methods for intravascular local drug delivery.

Other designs including bi-material kirigami surfaces that include plastic hinges to provide out of plane popping motion and insoluble drug-loaded needle tips for injection and deposition of drug depots by dissolution into the mucosa could improve delivery performance, and importantly, reduce the risk of tissue inflammation as well as safe, atraumatic removal. Moreover, given local drug exposure is increased considerably with submucosal injection, local pharmacokinetics will need to be characterized and optimized for the specific clinical application. This will likely inform the delivery of much lower total doses of the drug. As part of this evaluation potential drug loss in the presence of fluid in the lumen will also have to be characterized. This could present a greater challenge in the vasculature and potentially require transient occlusion of the proximal vessel. Future successful translation of these technologies will involve further in vivo testing of intraluminal kirigami stents with the aforementioned improved designs, optimization of manufacturing processes, optimal formulation development and evaluation of a range of deposition systems (e.g. coating vs microfluidics), and evaluation of sustained release within a target therapeutic range across different drug types depending on the target application sites.

References

1. Brem, H., Kader, A., Epstein, J., Tamargo, R. J. , Domb, A., Langer, R., Leong, K. W. Biocompatibility of a biodegradable, controlled-release polymer in the rabbit brain. *Sel Cancer Ther.* 5(2): 55-65 (1989).
2. Shatzel, J. *et al.* Drug eluting biliary stents to decrease stent failure rates: A review of the literature. *World J Gastrointest. Endosc.* 8(2): 77-85 (2016).
3. Kong, Y. *et al.* Preparation and characterization of paclitaxel-loaded poly lactic acid-co-glycolic acid coating tracheal stent. *Chin Med J (Engl)* 127(12): 2236-40 (2014).
4. Zhang, S. An inflammation-targeting hydrogel for local drug delivery in inflammatory bowel disease. *Sci. Transl. Med*. 7(300): 300ra128 (2015).
5. Kearney, C. J., & Mooney. D. J. Macroscale delivery systems for molecular and cellular payloads. *Nat. Mater.* 12, 1004–1017 (2013).
6. Stefanini, G.G., & Holmes, D.R. Drug Therapy: Drug-eluting coronary-artery stents. *The New England Journal of Medicine* 368(3): 254 (2013).
7. Martins, B., Retes, F., Medrado, B., Lima, M., Pennacchi, C., Kawaguti, F., Safatle-Ribeiro, A., Uemura, R., & Maluf-Filho, F. Endoscopic management and prevention of migrated esophageal stents. *World J Gastrointest Endosc.* 6(2): 49–54 (2014).
8. Lee, P., Moore, R., Raizada, A., & Grotz, R. Small bowel perforation after duodenal stent migration: An interesting case of a rare complication. *World J Radiol.* 3(6): 152–154 (2011).
9. Nelson, D. B., Bosco, J. J., Curtis, W. D., Faigel, D. O., Kelsey, P. B., Leung, J. W., Mills, M. R., Smith, P., Tarnasky, P. R., VanDam, J., Wassef, W. Y. Technology status evaluation report: Injection Needles. *Gastrointest Endosc.* 50(6): 928-31 (1999).
10. Chung, S. S., Lau, J. Y., Sung, J. J., Chan, A. C., Lai, C. W., Ng, E. K., Chan, F. K., Yung, M. Y., & Li, A. K. Randomised comparison between adrenaline injection alone and adrenaline injection plus heat probe treatment for actively bleeding ulcers. *BMJ* 314: 1307-11 (1997).
11. Soehendra, N., Bohnaker, S., Binmoeller, K. F. Nonvariceal Upper Gastrointestinal Bleeding. New and alternative hemostatic techniques. *Gastrointest Endosc Clin North Am* 7:641-57 (1997).
12. Pang,Y., Liu, J., Moussa, Z. L., Collins, J. E., McDonnell, S., Hayward, A. M., Jajoo, K., Langer, R., & Traverso, G. Endoscopically Injectable Shear-Thinning Hydrogels Facilitating Polyp Removal. *Adv. Sci.* 30 6(19): 1901041 (2019).
13. Usman, R. M., Jehangir, Q., & Bilal, M. Recurrent Esophageal Stricture Secondary to Pemphigus Vulgaris: A Rare Diagnostic and Therapeutic Challenge. *ACG Case Rep J.* 6(2), 2019.
14. Swaminath, A., & Lichtiger, S. Dilation of Colonic Strictures by Intralesional Injection of Infliximab in Patients With Crohn's Colitis. *Inflamm Bowel Dis.* 14(2): 213-6 (2008).
15. Rafsanjani, A., Zhang, Y., Liu, B., Rubinstein, S. M. & Bertoldi, K. Kirigami skins make a simple soft actuator crawl. *Sci. Robot.* 3, eaar7555 (2018).
16. Tang, Y., Li, Y., Hong, Y., Yang, S., Yin, J. Programmable active kirigami metasheets with more freedom of actuation. *Proceedings of the National Academy of Sciences*, 2019; 201906435.
17. Fu, H., Nan, K., Bai, W. et al. Morphable 3D mesostructures and microelectronic devices by multistable buckling mechanics. *Nat. Mater.* 17, 268–276 (2018).

18. Yusuke Morikawa et al, Donut-Shaped Stretchable Kirigami: Enabling Electronics to Integrate with the Deformable Muscle, *Adv. Health. Mate.* (2019).
19. Shyu, T. C. *et al.* A kirigami approach to engineering elasticity in nanocomposites through patterned defects. *Nat. Mater.* 14, 785–789 (2015).
20. Zheng, W. *et al.* Kirigami-Inspired Highly Stretchable Nanoscale Devices Using Multidimensional Deformation of Monolayer MoS 2. *Chem. Mater.* 30, 6063–6070 (2018).
21. Liu, Z. *et al.* Nano-kirigami with giant optical chirality. *Sci. Adv.* 4, 1–8 (2018).
22. Wu, C., Wang, X., Lin, L., Guo, H. & Wang, Z. L. Paper-Based Triboelectric Nanogenerators Made of Stretchable Interlocking Kirigami Patterns. *ACS Nano* 10, 4652–4659 (2016).
23. Rafsanjani, A. & Bertoldi, K. Buckling-Induced Kirigami. *Phys. Rev. Lett.* 118, 1–11 (2017).
24. P. Celli, C. McMahan, B. Ramirez, A. Bauhofer, C. Naify, D. Hofmann, B. Audoly, C. Daraio. Shape-morphing architected sheets with non-periodic cut patterns. *Soft Matter* 14, 9744 (2018).
25. Y. Zhang, Z. Yan, K. Nan, D. Xiao, Y. Liu, H. Luan, H. Fu, X. Wang, Q. Yang, J. Wang, W. Ren, H. Si, F. Liu, L. Yang, H. Li, J. Wang, X. Guo, H. Luo, L. Wang, Y. Huang, J. A. Rogers. A mechanically driven form of Kirigami as a route to 3D mesostructures in micro/nanomembranes. *Proc. Natl. Acad. Sci. USA* 112, 11757 (2015).
26. Babaee, S., Pajovic, S., Rafsanjani, A., Shi, Y., Bertoldi, K., & Traverso, G. Bioinspired kirigami metasurfaces as assistive shoe grips. *Nat. Biomed. Eng.* (2020).
27. Connolly F, Polygerinos P, Walsh CJ, Bertoldi K. Mechanical programming of soft actuators by varying fiber angle. *Soft Robot* 2(1): 26–32 (2015).

Acknowledgement

We would like to thank Prof. R. Langer for helpful discussion and support. We would like to thank V. Spanoudaki and W. Huang for help with the micro-CT and histology images, A. Rafsanjani for productive discussions, and all colleagues of the Langer and Traverso Laboratories for fruitful discussions.

Authors Contributions

S.B., Y.S., and G.T. conceived and designed the research. S.B. and Y.S. performed the design, FE simulations, manufacturing, mechanical characterization, and in vitro testing of the stent prototypes. S.T., J.E.C., K.I., A.M.H., M.A., S.B., and Y.S. performed the in vivo pig experiments. S.A. performed particle synthesis and characterization. K.H. and A.L. performed biochemistry analysis. S.B., Y.S., S.A., M.W., M.A., and G.T. discussed and analyzed the results and wrote the manuscript. All authors reviewed the manuscript and provided active and valuable feedback.

Competing Interests

This work was funded in part by: the Karl van Tassel (1925) Career Development Professorship and the Department of Mechanical Engineering, MIT. S.B., Y.S., S.A., M.A., and G.T. are co-inventors on provisional patent applications for the technology described. The remaining authors disclose no competing financial interests. Complete details of all relationships for profit and not for profit for G.T. can be found at the following link: https://www.dropbox.com/sh/szi7vnr4a2ajb56/AABs5N5i0q9AfT1IqIJAE-T5a?dl=0.

Reporting Summary

Further information on research design is available in the Nature Research Reporting Summary linked to this article.

Data availability

All the data supporting the results in this study are available within the paper and its Supplementary Information. Source data generated in this study and used to make the figures are provided.

Code availability

Abaqus scripts used for the numerical analyses are available from the corresponding author upon request.

Figures

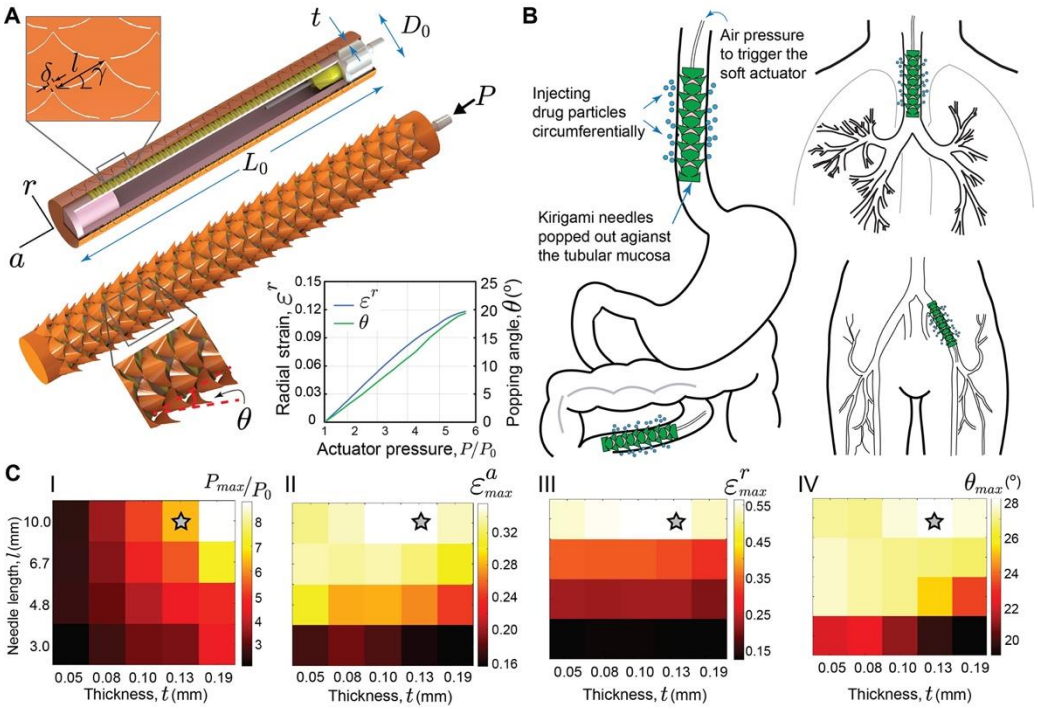

Figure 1. Overview and numerical characterization of injectable kirigami-based stents. (**A**) Schematic illustration of the stent system in the undeformed and deployed configurations, consisting of the pneumatic soft actuator integrated with a kirigami shell characterized with needle length (l), cut angle (γ), hinge length (δ), and needle thickness (t). L_0 and D_0 are the initial length and outer diameter of the stent. The evolution of radial expansion (ε^r) and popping angle (θ) of the stent by 0.12 and 20° through applying external pressure up to 5.8 atm for the illustrated stent design with initial length $L_0 = 8$ cm and outer diameter $D_0 = 11.2$ mm. (**B**) Schematic of deployment of the injectable kirigami-based stent in the tubular segments of the GI tract, trachea, and iliac artery. (**C**) Effect of l and t on the maximum actuator pressure (P_{max}/P_0, P_0 =1 atm), maximum axial (ε^a_{max}) and radial (ε^r_{max}) strains, and maximum popping angle (θ_{max}) of the stent with $L_0 = 8$ cm and $D_0 = 12.5$ mm. The star marker indicates the final fabricated esophageal stent prototype.

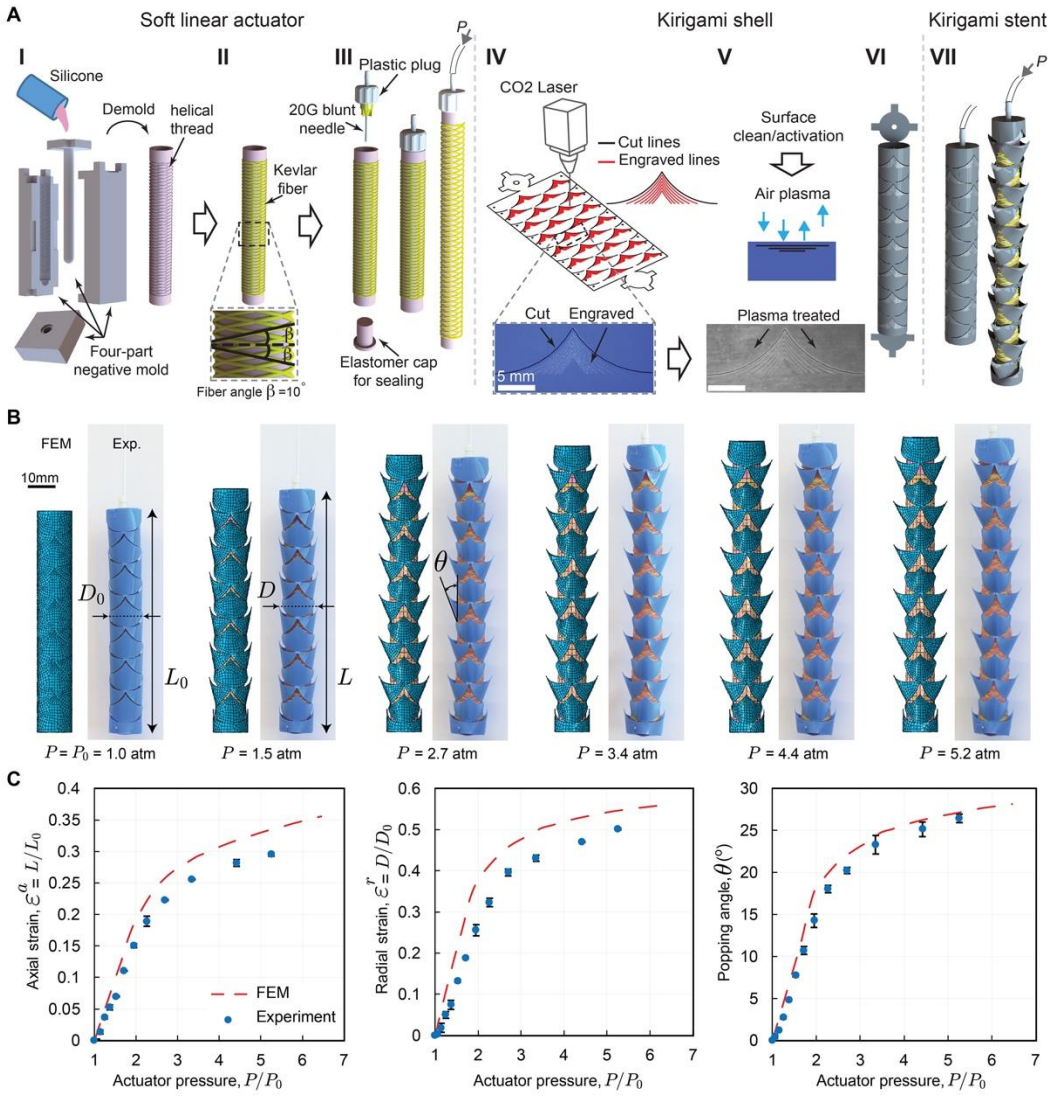

Figure 2. Stent fabrication and mechanical characterization of the esophageal stent prototypes. (**A**) The kirigami-based stents are manufactured in eight steps: (I) cast silicone-based rubber, (II) fiber reinforce using Kevlar fibers, (III) seal and assembly, (IV) laser cut and laser engrave, (V) plasma surface treat, (VI) bond kirigami shell, and (VII) assemble the actuator and kirigami shell. The insets in IV and V are the micrographs of a representative kirigami needle surface. Similar results were obtained for $n = 6$ independent samples. (**B**) Numerical and experimental images of the esophageal stent at different levels of actuator pressure, P = 1.0, 1.5, 2.7, 3.4, 4.4, and 5.2 atm. L_0 = 8 cm and D_0 = 12.5 mm are the initial length and outer diameter, and L, D, and θ are the length, outer diameter, and popping angle of the stent for a given P, respectively. The kirigami is 80 × 43 mm surface consists of a periodic array of 2 ×13 = 26 stretchable needles. (**C**) Evolution of axial strain (ε^a), radial strain (ε^r), and popping angle (θ) were plotted as a function of P/P_0. Numerical predictions (red dashed line) are compared to experimental (blue markers) results. The markers represent the mean ± SD for n =3 prototypes across the 22 needles per each stent.

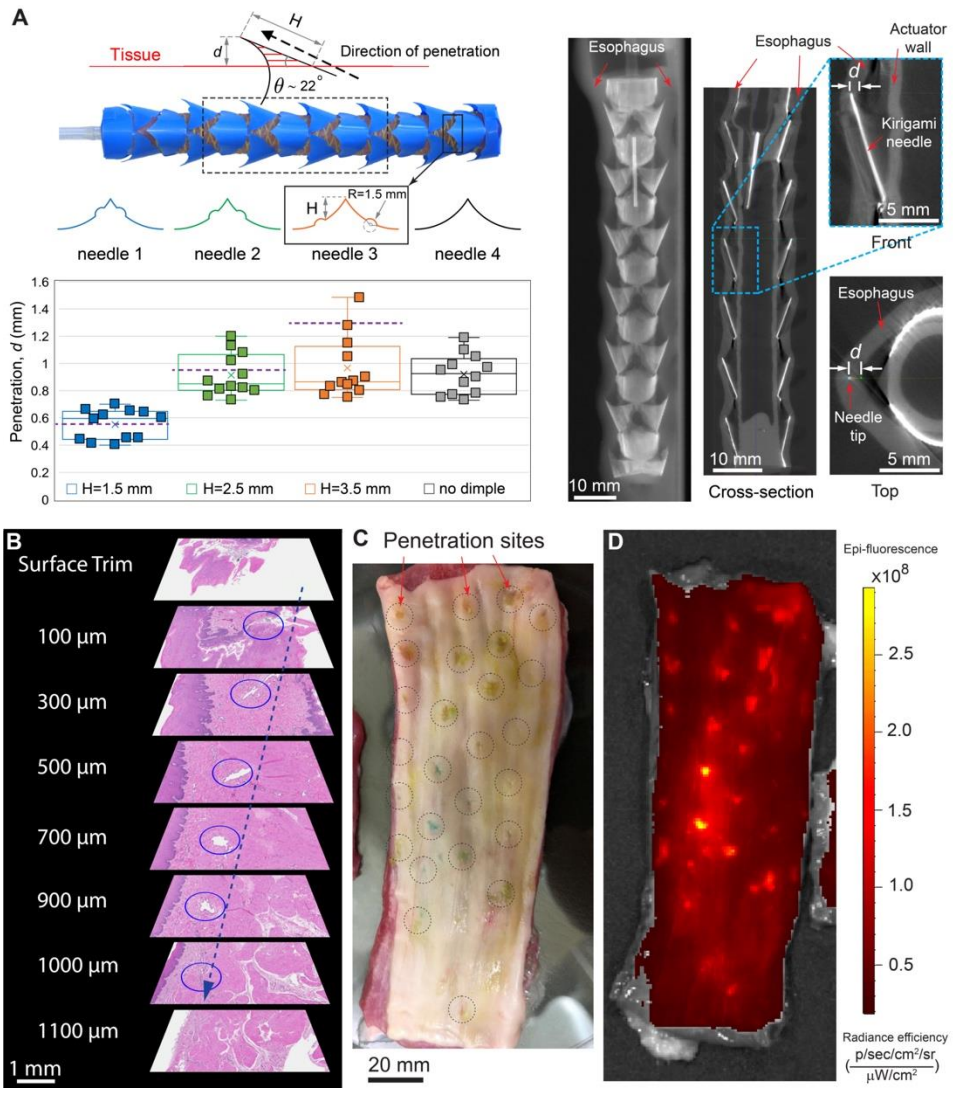

Figure 3. Ex vivo and in vivo evaluation of controlled penetration of the stent needles to the esophageal tissue. (**A**) Ex vivo representative 3D micro-CT scanned image of the stent deployed in the esophagus. 2D cross-sectional slices from the front and top views were used to obtain the penetration depth within the tissue (d) for the stent needles with effective lengths H =1.5 mm (needle 1 in blue), 2.5 mm (needle 2 in green), 3.5 mm (needle 3 in orange), and control (needle 4 in black) reported in the plot. The arc-shaped features (i.e., dimples with R = 1.5 mm) were incorporated on the two sides of the needles. Data are presented as median ± 25 to 75% confidence interval (boxes) with the smallest and largest values (whiskers) for n = 12 middle needles (inside the dashed rectangle). The × markers indicate the mean values. The dashed lines are the expected penetration depth, $d_{max} = H \sin\theta$, where θ~ 22° is the maximum popping angle considering the surrounding tissue wall. (**B**) Representative in vivo histological images of an esophageal tissue showing 1.09 ± 0.16 mm penetration of needles without perforation (mean ± SD, n = 3). (**C**) Optical image of the penetration sites taken after in vivo deployment of the stent (blue spots are food-grade color used in coating formulation). Similar results were obtained for n = 3 independent samples. (**D**) In vivo 2D epi-fluorescence visualization of deposited fluorescent microparticles in the esophageal tissue acquired by an IVIS (in vivo imaging system) SpectrumCT. Similar results were obtained for n = 3 independent samples.

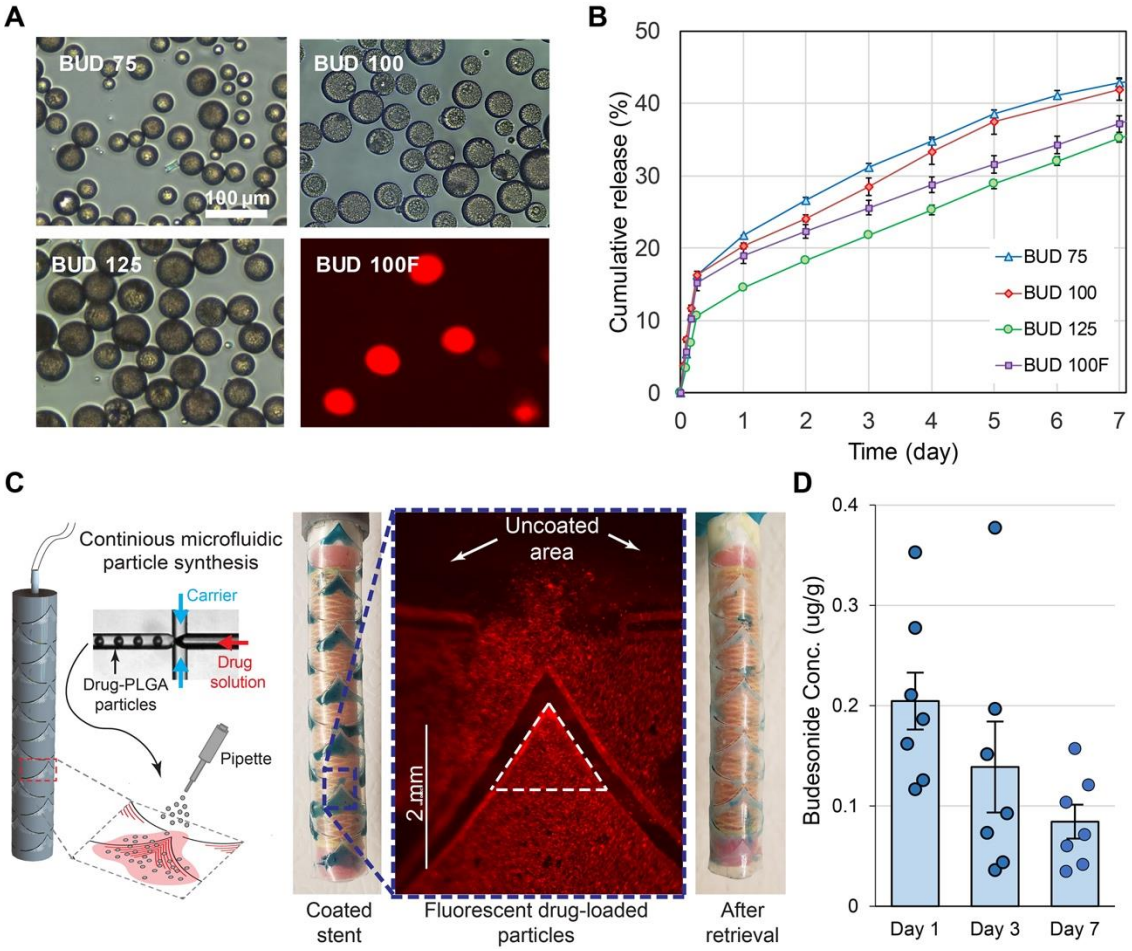

Figure 4. In vivo extended drug release through deposition of drug-loaded polymeric particles. (**A**) Optical microscope images of budesonide loaded PLGA microparticles with different concentrations of budesonide including 75, 100, and 125 mg/ml denoted by BUD 75, BUD 100, BUD 125, respectively. BUD 100F corresponds to 100 mg/ml concentration of fluorescent budesonide-PLGA particles. Similar results were obtained for $n = 5$ independent samples per concentration. (**B**) In vitro cumulative release profile of budesonide encapsulated on PLGA microparticles across different formulations incubated in 37°C PBS for 7 days (mean ± SD, $n = 3$). (**C**) Kirigami stent needles were coated via pipetting BUD 100F particle solution, synthesized using a continuous microfluidic droplet generation method. The images of the coated stent before and after deployment, as well as a magnified view of coated needles (taken by a fluorescence microscope) are presented. Similar results were obtained for $n = 10$ independent samples. (**D**) Concentration of budesonide delivered to the esophageal tissue through in vivo deployment of the coated stent at three different time points Day 1, Day 2, and Day 7 (mean ± SE, for $n = 7$).

Methods

Numerical simulations

All the simulations were carried out using the commercial Finite Element (FE) package Abaqus 2017 (SIMULIA, Providence, RI). The Abaqus/Explicit solver was employed for the simulations. We constructed FE models of the elastomer actuator, Kevlar fiber, nylon plastic plug, and kirigami plastic shell (imported from SolidWorks) to investigate the deformation response of the kirigami stent.

We used a linear elastic material model for Kevlar fiber, polyester plastic, and nylon plastic. Kevlar fiber has a density of 1.13E3 kg/m3, Young's modulus of 31067 MPa, and Poisson's ratio of 0.36 with a

circular beam section of 0.0889 mm radius. Polyester plastic sheet has a density of 1.13E3 kg/m3, Young's modulus of 3655 MPa, Poisson's ratio of 0.4 with shell section of 0.127 mm thickness. The nylon Plastic has a density of 1.15E3 kg/m3, Young's modulus of 4000 MPa, and Poisson's ratio of 0.36. The constitutive behavior of the elastomer was captured using a nearly-incompressible Neo-Hookean hyperelastic model (Poisson's ratio of ν_0 = 0.499 and density of 1000 kg/m3) with directly imported uniaxial test data.

Different element types were used to construct the three-dimensional (3D) FE models of the kirigami stent. Linear beam element (Abaqus element type B31, seed size=1) for the Kevlar fibers, 3D shell element with reduced integration (Abaqus element type S4R, seed size=1) for the plastic kirigami, and 3D brick element (Abaqus element type C3D8, seed size=1.5) for the elastomer actuator and the plastic plug. The Dynamic Explicit solver with a time period of 500 and a mass scaling factor of 1000 (to facilitate convergence) was used. TIE constraint (surface to surface) was applied between the fibers and the elastomeric body. General Contact type interaction with penalty friction coefficient 0.2 for tangential behavior and "hard" contact for normal behavior were applied. Finally, the pressure load applied to the inner surface of the linear actuator using SMOOTH step amplitude curve, and the deformation of the kirigami stent model was monitored as a function of the applied pressure.

Kirigami surface manufacturing

The plastic kirigami surfaces were manufactured through laser cutting the polyester plastic shim stock using a CO_2 Universal Laser Systems PLS6.75. The cutting parameters were 35% power, 100% speed, and 250 PPI. The etching parameters for the raster lines on the needles were 20% power, 100% speed, and 250 PPI. The dimension of the kirigami prototypes used for this study was Length × Width = 80 mm × 43 mm composed of a periodic array of 2 ×13 = 26 stretchable needles with l= 10.0 mm, δ=1.3 mm, and φ=30°, shown in Supplementary Figures 6A and 6B. The needles were barb-shaped with a radius of curvature ρ=10.05 mm with six raster lines engraved over the needles' surface (with 0.5 mm spacing) to improve the adhesion between the plastic surface and the coating layer. Small holes perforated along the two sides of the sheet, which will be used to facilitate alignment.

Finally, the kirigami surface was glued into a cylindrical-shaped shell using Loctile® Plastic Bonding adhesive (Henkel Corp), facing the surface with engraved raster features outward (Supplementary Figure 6C). The adhesive was applied only at overlapping areas where the small holes on the two sides of the surface were aligned.

Fluid-powered soft linear actuator manufacturing

An elastomeric cylindrical-shaped actuator with the length of 70 mm, circular cross-section with outer diameter 10mm, and wall thickness 1.5 mm was fabricated using a casting approach. First, four-part negative mold was designed in SolidWorks 2017 and fabricated using a 3D printer (Object30 Pro, Stratasys Ltd) out of Vero Clear rigid plastic with a glossy finish (Supplementary Figure 5). All the molds were sprayed with a releasing agent (Universal Mold Release, Smooth-On) for easy demolding. Then, the elastomeric actuator body and cap were cast separately using a silicone-based rubber (vinylpolysiloxane (a-silicone) duplicating elastomer with commercial name Elite Double 8, Zhermack SpA, Italy). The casted mixture was mixed for two minutes, placed in a vacuum for degassing, and was allowed to set at room temperature for thirty minutes to cure.

After demolding, the actuator body was looped with stiff Kevlar fibers ($r = 0.0889$ mm, Kevlar Sewing Thread, SGT KNOTS supply Co, NC) along the helical thread pattern, which was incorporated in the design for the fiber alignment (Figure 2A and Supplementary Figure 5). The fibers constrain the deformation of the actuator in the radial direction, leading to the creation of an extensional actuator[27]. Note that the 0° circular pattern will constraint the radial expansion and produce a pure extensional balloon. However, we introduced a helical pattern of 4 sets of clockwise 10° and 4 sets of mirrored counter-clockwise 10° fibers, which together led to a pure extension performance. Using finite element (FE) simulation and experiments, we evaluated the deformation response of the fluidic actuator demonstrating 0.5 axial strain by applying 2.2 atm pressure (Supplementary Video S4).

Next, a uniform thin layer of a silicone adhesive (Sil-Poxy, Smooth-On, Inc) was applied to the outer surface of the fiber-reinforced actuator body to enhance the bonding between the fiber and elastomer. The extensional actuator body was left in the room temperature for 30 min, allowing the silicone adhesive to dry. Then, the final linear actuator was assembled by attaching the elastomeric cap to one end of the actuator body, and a 20G blunt needle (Braintree Scientific, Inc) and a nylon plastic quick-turn plug (McMaster-Carr, part#51525K121) to the other end. Both ends were fully sealed using the silicone adhesive. A 50 ml syringe, connected to the plug via a Tygon PVC clear tubing (ID=1.59 mm, OD=3.18 mm), was used for inflation (actuation) of the soft linear actuator.

Plasma surface treatment

Plasma treatment was used to micro clean and alter the surface properties of the kirigami surfaces for adhesion improvement. The kirigami surfaces were treated in air plasma with high radio frequency at 500 mTorr for 1h using a plasma cleaner device (High power expanded cleaner, PDC-001-HP, Harrick Plasma). That results in the creation of hydrophilic surfaces and improvement in adhesive bond to the drug-coated films that facilitates the drug solution coating and enhances the drug film stability.

Ex vivo measurement of the controlled depth of penetration

Conductive ink coating

To make the external surface of kirigami stent (especially the needles) radiopaque, the flat kirigami surfaces were coated with a thin layer of tungsten filled conductive ink (RO-948 Radio Opaque Ink, MICROCHEM) using a roller. The coated kirigami surface was left overnight to dry.

Ex vivo testing of kirigami stent

The radiopaque stent prototypes with different needle's lengths (H) were deployed in the esophagus harvested from a Yorkshire pig 30 minutes after euthanasia. The method of euthanasia was approved in the MIT Committee on Animal Care protocol. Pigs are anesthetized prior to euthanasia with an intravenous (IV) administration of sodium pentobarbital (~ 100 mg/kg). The esophagus was rinsed for approximately 10 sec under running tap water to wash away contaminants such as gastric fluid. To deploy the stent, a custom 3D printed fixture was used. The fixture consisted of a 20 mm diameter tube 3D printed (Objet30 Pro, Stratasys) out of VeroClear plastic (product number: RGD810, Objet). The 20 mm tube was placed inside the *ex vivo* esophagus to hold it open for deployment, and the stent with a given needle's length inserted into the esophagus via the tube. Once it reached the proximal esophagus, the linear actuator inside the stent was inflated by pumping air using a plastic syringe connected to the stent via a Tygon PVC clear tubing results in popping up the needles. A syringe stopcock was used to maintain the pressure inside the stent's actuator and keep all the needles popped up at the maximum angle (~22°) against the surrounding esophageal tissue. The kirigami needles were inserted into the tissue by gently pulling the Tygon tubing backward via application of ~ 8 N force.

Micro-Computed Tomography (Micro-CT) imaging

The deployed stent in the esophagus was then transferred into the micro-CT scanner (GE eXplore CT 120 scanner, General Electrics) and scanned following the protocol for soft tissue. Using the image viewer software (MicroView, Parallax innovations, ON, Canada), the penetration of the needles into the tissue was monitored by taking tomographic images at multiple views. The penetration depths were measured using both the cross-section and top views, where we were able to see the needle tips penetrated to the esophageal submucosa. The precise depths were obtained through measuring the distance between the inner surface of the tissue and the tip of the needles, *d*, as shown in Figure 3A.

In vivo delivery, deployment and removal of kirigami-based stents

The kirigami stent prototypes were deployed for in vivo evaluations in a large animal model (50 to 80 kg female Yorkshire pigs ranging between 4-6 months of age). The pigs were provided from Cummings School of Veterinary Medicine at Tufts University, Grafton, Massachusetts. The pig model was selected

for optimization and evaluation of the kirigami stent system given its known similarities in dimensions to adult human anatomy and has been widely used in the evaluation of biomedical GI devices[28,29]. Following 24 hours of liquid diet and overnight fasting, the animal was sedated with Telazol (tiletamine/zolazepam, 5 mg/kg intramuscular (IM)), xylazine (2 mg/kg IM), and atropine (0.04 mg/kg IM) followed by endotracheal intubation and maintenance anesthesia with inhaled 2% soflurane (1-3% in oxygen). All animal experiments were conducted in accordance with protocols approved by the Committee on Animal Care at the Massachusetts Institute of Technology. An overtube (with $D_{\mathrm{in}} = 15.785$ mm and $D_{\mathrm{out}} = 19.05$ mm), with endoscopic guidance, was placed into the proximal esophagus to assist with the placement of the stent. The stent with 8 cm length and 12.5 mm diameter was inserted into the esophagus via the overtube pushed by the end of a scope. Once it reached the proximal esophagus, the overtube was removed, resulting in exposure of the stent to the esophageal mucosa. Similar to the ex vivo deployment, the linear actuator inside the stent was actuated by pumping air using a plastic syringe connected to the stent via a Tygon PVC clear tubing caused buckling up the needles. A syringe stopcock was used to maintain the pressure inside the fluidic actuator and keep all the needles popped up against the mucosa. The kirigami needles were then inserted into the submucosa by gently pulling the Tygon tubing backward via application of ~ 8 N force. After deployment, the stent was left in place for two minutes before retrieval. The stent was then retracted by releasing the actuator pressure that makes the needles to buckle in and recover its original shape for easy removal.

The animal was then euthanized using sodium pentobarbital at approximately 100~120 mg/kg via IV and the esophagus harvested after about 2 hours in compliance with the AVMA Guidelines on Euthanasia[30] and approved in the MIT Committee on Animal Care protocol.

Histology

Histological analysis was performed on tissue biopsies to characterize the depth of penetration. Biopsies were taken at the penetration sites of the harvested esophagi, where needles coated with tissue marking dye (product number: 0736-3, Cancer Diagnostics, Inc.) penetrated. The biopsies were fixed in formalin fixative (Sigma Aldrich) for 24 hours before transfer to 70% ethanol. Tissue samples were then embedded in paraffin, cut into 5 μm-thick tissue sections, stained with haematoxylin and eosin, and imaged using an Aperio AT2 Slide Scanner (Leica Biosystems).

Endovascular injectable kirigami stents

A 20 or 22F vascular introducer sheath (Medtronic) was percutaneously placed in the femoral artery of the pig under ultrasound and fluoroscopic guidance. The pig was then systemically heparinized with unfractionated heparin (100u/kg). In the contralateral femoral artery, a 12F vascular introducer sheath was placed and a 32mm Coda balloon (Cook Medical) was positioned in the descending aorta via the 12F sheath. After balloon occlusion of the descending aorta with the Coda balloon, the kirigami stent with 7 cm length and 5.5 mm diameter and coated with tissue marking dye (product number: 0736-3, Cancer Diagnostics, Inc.) was pre-loaded into a 18F vascular introducer that was then inserted through the previously placed 20F sheath positioned in the iliac artery (“sheath-in-sheath” approach). The kirigami stent device was then unsheathed in the iliac artery, inflated, and was gently retracted to engage the arterial wall. A syringe stopcock was used to maintain the pressure inside the stent’s fluidic actuator and keep all the needles fully expanded at the maximum angle ~22° against the surrounding vascular tissue. After two minutes, the kirigami device was deflated and removed. The pig was then sacrificed and the iliac artery was harvested for histopathological evaluation.

Preparation of coating solutions for spray coating of kirigami stent

Fluorescent magnetic polystyrene microparticles (Fluorescent Nile Red Magnetic Particles,1.0% w/v, 4.0-4.9 μm nominal size, Catalog No. FPM-4056-2**,** Spherotech, US) and 25% w/v of Dextran sulfate sodium salt in double-distilled H2O Water were mixed with a ratio of 5:2. 10% w/w of glycerol as a plasticizer was added to the mixture. The final mixture was vortexed for 10 minutes before coating.

In vivo testing of kirigami stents for fluorescent particles delivery

The kirigami stent prototypes coated with fluorescent polystyrene microparticle solution (see “Preparation of coating solutions for spray coating of kirigami stent”) were used for in vivo evaluation of polymeric particle delivery in the esophagus of a female Yorkshire pig. The method of delivery, deployment and removal were the same as described in “In vivo delivery, deployment and removal of kirigami-based stents”. After euthanasia, the fluorescent red magnetic particles deposition in the harvested esophagus was assessed by taking a 2D epi-fluorescence image using an IVIS (in vivo imaging system) Spectrum in vivo imaging system (PerkinElmer) at fluorescent excitation and emission filter set of 570 nm and 620 nm, respectively.

Continuous microfluidic synthesis of budesonide-PLGA microparticles

Budesonide-PLGA [Poly(D,L-lactide-co-glycolide) ester terminated, lactide:glycolide 75:25, Mw 76,000-115,000, Sigma Aldrich] microparticles were synthesized using a continuous microfluidic drug-PLGA droplet generation method, shown in Supplementary Figure 12. We used a one reagent glass 3D flow-focusing microfluidic chip with hydrophilic surface and 100µm deep channels (Dolomite, UK) followed by a solvent extraction step. Two partially miscible solvents including dichloromethane (DCM, Sigma Aldrich) and water were used as drug solvent/carrier and droplets carrier phases, respectively. Budesonide (75,100, and 125 mg/ml) and 1% w/v PLGA were dissolved in DCM as an organic fluid. 2% w/v PVA in double-distilled water was used as an aqueous/carrier phase for droplet generation. All fluids passed through a 0.2 µm pore microfilter before droplet production. To generate fluorescence-sensitive budesonide-PLGA particles, 0.3% w/v of PLGA-SH (LG 50:50, PolySciTech) and 20µl of Alexa Flour 647 C2 Maleimide dye (Invitrogen) was also added to the budesonide-PLGA solution. The microfluidic system set-up includes two pressure pumps (Mitos P-Pump, Dolomite Microfluidics) equipped with in-line Mitos Flow Rate Sensors to monitor and control the streams flow rates. Two flow rate sensors, 30 - 1000 µl/min and 1 - 50 µl/min, were employed in the organic line and aqueous line, respectively. An air compressor (California air tools) provide the supply pressure for the P-Pumps at 400 KPa working pressure. The pumps were connected to 30/400 ml and 30ml volume remote pressure chambers placed on magnetic stirrer for continuous mixing and delivering of PVA in water and DCM-PLGA-Budesonide solution to the chip with 10 µl/min aqueous/carrier rate and 1.35 µl/min organic/drug-PLGA solutions rate, respectively. The particle synthesis process was continuously continued to reach 500 mg of particles while the DCM solvent was evaporating/ by connecting the particle’s collection siliconized stirred vessel to very mild vacuum pressure (about 650 Torr). The drug/polymer ratio and microfluidic chip running parameters were optimized to achieve highly homogenous microparticles for deposition on the kirigami stent. We synthesized three formulations of budesonide-PLGA particles with 75,100, and 125 mg/ml concentration of budesonide, denoted by BUD75, BUD100, and BUD125, respectively. Additionally, we synthesized 100 mg/ml concentration of fluorescent budesonide-PLGA particles (BUD 100F) via addition of Alexa Flour 647 C2 Maleimide as described.

Characterization of budesonide-PLGA particles

Particle size

The size of the prepared formulations for the drug-loaded particles (BUD 75, BUD 100, BUD 125, and BUD 100F) was measured for an average of 80 particles (Supplementary Figure 13). A digital camera equipped with an optical microscope (EVOS XL, Thermo Scientific) used to visualize the particles, and counted by Nikon NIS-Elements advanced image analysis software.

Quantifying the drug content of particles

About 9-11 mg of microparticles (MPs) in 3 replicates were suspended and dissolved in 0.5 ml of acetonitrile by vortexing for 5 min. Then, 500 µl of the solution with 5-fold dilution were prepared and drug concentration in the replicates was measured using HPLC analysis (High Performance Liquid Chromatography) described in Methods. The obtained HPLC data were used to calculate drug loading and encapsulation efficacy parameters reported in Supplementary Figure 13.

Drug loading (%) = [mass of budesonide (mg) in MPs] / [mass of MPs (mg)] $\times 100$

Encapsulation efficiency (%) = [mass of budesonide (mg) in MPs] / [theoretical mass of budesonide (mg) added initially] $\times$ 100 [31]

High-performance liquid chromatography analysis of drug release

Budesonide kinetic release studies were analyzed using High-Performance Liquid Chromatography (HPLC). A 1260 Infinity II HPLC system (Agilent Technologies Inc., USA) equipped with a 1260 quaternary pump, 1260 Hip ALS autosampler, 1290 thermostat, 1260 TCC control module, and 1260 diode array detector. Data processing and analysis was performed using OpenLab CDS software (Agilent Technologies Inc., USA).

Budesonide chromatographic isocratic separation was carried out on an Agilent 4.6 x 150 mm Zorbax Eclipse XDB C-18 analytical column with 5 µm particles, maintained at 30°C. The optimized mobile phase consisted of 20 mM dipotassium phosphate buffer (pH 3.00 adjusted with phosphoric acid) and acetonitrile [30:70 (v/v)] at a flow rate of 1.00 mL/min over a 5 min run time. The injection volume was 5 µl, and the selected ultraviolet (UV) detection wavelength was 244 nm at a bandwidth of 4.0, no reference wavelength, and an acquisition rate of 40 Hz.

In vitro release of budesonide-PLGA microparticles

The in vitro release of budesonide from microparticles was performed using a horizontal shaker with 200 rpm speed at 37ºC (Innova Shaker, New Brunswick). PBS [phosphate buffered saline (pH 7.4 (1X) Gibco, Thermo Fisher Scientific] was selected as the in vitro medium for drug release kinetics characterization given the intent to target the submucosal environment where extracellular fluid with a similar pH would be encountered. 3 to 5 milligrams of budesonide loaded microparticles were added to 1 ml PBS with 0.1% Tween 20. Experiments were performed at 37°C and samples were taken at 2, 4, 6 h, and then daily up to 7 days of release. Buffer were refreshed at different time intervals and the drug content was analyzed using HPLC analysis of 500 µl of supernatant solution described in Methods.

Coating the kirigami stent needles using budesonide-PLGA microparticles

100 mg/ml concentration of fluorescent budesonide-PLGA particles (BUD 100F) was used to coat the needles of the kirigami stents by pipetting 20 µl of the solution two times per needle with 5h interval for drying at room temperature. Coated kirigami stents were kept in a door cap tightened 50 ml tube at -20˚C deployment procedure. The Figure 4C shows a kirigami needle loaded with BUD 100F taken by EVOS XL fluorescence imaging system (Thermo Scientific).

In vivo testing of kirigami stents for prolonged delivery of budesonide-PLGA particles

To evaluate the ability of kirigami stents, loaded with the budesonide-PLGA microparticles, to achieve long-term delivery, we administered them to a large animal model (three Yorkshire pigs). The details of delivery, deployment and removal of the stents were the same as fluorescent particle-loaded stents described in “In vivo testing of kirigami stents for fluorescent particles delivery”. The three animals were euthanized at three different time points: 1 day, 3 days and 7 days after deployment/removal in compliance with the AVMA Guidelines on Euthanasia (*3*). Endoscopic evaluation of the esophagus over the course of the study were performed to further explore the esophagus and ensure the absence of any ulceration or injury (Supplementary Video S9). The esophagi of three pigs were harvested 10 minutes after euthanasia. 8 mm diameter biopsies were used to take biopsies at least seven needle penetration sites per retrieved esophagus. The penetration sites were recognized by using an IVIS Spectrum in vivo imaging system (PerkinElmer). Note that the drug-loaded particles (BUD 100F) were fluorescence-sensitive due to incorporation of Alexa Flour 647 C2 Maleimide (Invitrogen). The biopsies were then frozen until extraction. Budesonide was extracted from esophageal tissue by placing each biopsy in 500 µl of 5% BSA in PBS and homogenizing two times by 6500 rpm for 30 seconds. A 100 µl fraction of the homogenate was collected. 50 µl of 5 µg/ml hydrocortisone (internal standard) in acetonitrile and 1mL ethyl acetate was added for budesonide extraction. These samples were vortex and centrifuged for ten minutes at 13000rpm. Following centrifugation, the supernatant was evaporated to dryness. Samples were reconstituted in 300 µl acetonitrile and 200 µl of the reconstitute were pipetted into a 96-well plate

containing 200 µl of Nanopure water and used for ultraperformance liquid chromatography–tandem mass spectrometry (UPLC-MS/MS) analysis.

UPLC-MS/MS analysis of budesonide delivery through needles

The analysis was performed on a Waters ACQUITY UPLC- I-Class System aligned with a Waters Xevo-TQ-S mass spectrometer (Waters Corp.). Liquid chromatographic separation was performed on an ACQUITY UPLC Charged Surface Hybrid C18 (50 mm × 2.1 mm, 1.7-µm particle size) column at 50°C. The mobile phase consisted of aqueous 0.1% formic acid and 10 mM ammonium formate solution (mobile phase A) and an acetonitrile: 10 mM ammonium formate and 0.1% formic acid solution [95:5 (v/v)] (mobile phase B). The mobile phase had a continuous flow rate of 0.6 ml/min using a time and solvent gradient composition. The initial composition (100% mobile phase A) was held for 1 min, after which the composition was changed linearly to 50% mobile phase A over the next 0.25 min. At 1.5 min, the composition was 20% mobile phase A, and at 2.5 min, the composition was 0% mobile phase A, which was held constant until 3 min. The composition returned to 100% mobile phase A at 3.25 min and was held at this composition until completion of the run, ending at 4 min, where it remained for column equilibration. The total run time was 4 min, and sample injection volume was 2.5 µl. The mass spectrometer was operated in the multiple reaction monitoring (MRM) mode. Sample introduction and ionization was by electrospray ionization (ESI) in the positive ionization mode. MassLynx 4.1 software was used for data acquisition and analysis.

Stock solutions of budesonide and internal standard hydrocortisone were prepared in methanol at a concentration of 500 µg/ml. A twelve-point calibration curve was prepared in methanol ranging from 1 to 5000 ng/ml.

Statistical analysis

All the experimental data were reported as mean ± standard deviation or mean ± standard error for n measurements for each group. n is stated in the figure captions.

Supplementary References

28. Y. Mintz, S. Horgan, J. Cullen, E. Falor, M. A. Talamini, Dual-lumen natural orifice translumenal endoscopic surgery (NOTES): a new method for performing a safe anastomosis. *Surg. Endosc.* 22, 348-351 (2008).

29. M. Tarnoff, S. Shikora, A. Lembo, Acute technical feasibility of an endoscopic duodenal-jejunal bypass sleeve in a porcine model: a potentially novel treatment for obesity and type 2 diabetes. *Surg. Endosc.* 22, 772-776 (2008).

30. S. Leary, W. Underwood, R. Anthony, S. Cartner, D. Corey, T. Grandin, C. Greenacre, S. Gwaltney-Brant, M. A. McCrackin, R. Meyer, D. Miller, J. Shearer, R. Yanong, *AVMA Guidelines for the Euthanasia of Animals: 2013 Edition* (American Veterinary Medical Association, Schaumburg, Illinois, 2013).

31. C. Gómez-Gaete, M. Retamal, C. Chávez, P. Bustos, R. Godoy, P. Torres-Vergara. Development, characterization and in vitro evaluation of biodegradable rhein-loaded microparticles for treatment of osteoarthritis. *European J. of Pharm. Sci.* 96, 390–397 (2016).